

# The distribution of metals in hot DA white dwarfs

N.J. Dickinson<sup>1</sup>, M.A. Barstow<sup>1</sup> and I. Hubeny<sup>2</sup>

<sup>1</sup>*Department of Physics & Astronomy, University of Leicester, Leicester LE1 7RH. UK.*

<sup>2</sup>*Steward Observatory, The University of Arizona, 933 N. Cherry Ave, Tucson, AZ 85721. USA.*

25 July 2018

## ABSTRACT

The importance to stellar evolution of understanding the metal abundances in hot white dwarfs is well known. Previous work has found the hot DA white dwarfs REJ 1032+532, REJ 1614-085 and GD 659 to have highly abundant, stratified photospheric nitrogen, due to the narrow absorption line profiles of the FUV N V doublet and the lack of EUV continuum absorption. A preliminary analysis of the extremely narrow, deep line profiles of the photospheric metal absorption features of PG 0948+534 suggested a similar photospheric metal configuration. However, other studies have found REJ 1032+532, REJ 1614-085 and GD 659 can be well described by homogeneous models, with nitrogen abundances more in keeping with those of white dwarfs with higher effective temperatures. Here, a re-analysis of the nitrogen absorption features seen in REJ 1032+532, REJ 1614-085 and GD 659 is presented, with the aim of better understanding the structure of these stars, to test which models better represent the observed data and apply the results to the line profiles seen in PG 0948+534. A degeneracy is seen in the modelling of the nitrogen absorption line profiles of REJ 1032+532, REJ 1614-085 and GD 659, with low abundance, homogeneously distributed nitrogen models most likely being a better representation of the observed data. In PG 0948+534, no such degeneracy is seen, and the enigmatically deep line profiles could not be modelled satisfactorily.

**Key words:** stars: abundances - atmospheres - white dwarfs - ultraviolet: stars

## 1 INTRODUCTION

As the end products of the lives of the vast majority of stars, a thorough understanding of white dwarfs is crucial to our understanding of stellar evolution. To understand the evolution of white dwarfs, accurate measurements of parameters such as the effective temperature of a star ( $T_{\text{eff}}$ , which gives how far along the cooling sequence the white dwarf has travelled) are required. A common technique (pioneered by Holberg et al. 1985 and extended to a large white dwarf sample by Bergeron et al. 1992) used to measure a white dwarf  $T_{\text{eff}}$  is to compare the observed Balmer line profiles to model calculations. The surface gravity ( $\log g$ ) of the star can be found in a similar way. Using these parameters as inputs to white dwarf evolutionary models (such as those of Wood 1995), one can then derive a stellar mass, which can then be used in studies of white dwarf mass distributions (e.g. Bergeron et al. 1992, Liebert et al. 2005), luminosity functions (e.g. Liebert et al. 2005) or initial-final mass relations (e.g. Casewell et al. 2009, Dobbie et al. 2009). Being among the oldest stellar objects, white dwarfs can be used as chronometers to age stellar populations (e.g. Fontaine et al. 2001); the age of the oldest white dwarf in the galactic disk can provide a lower age

estimate for the Milky Way. Reliable measurements of  $T_{\text{eff}}$  are therefore critical to our understanding of white dwarf stars and their application to stellar evolution.

For some time, it has been known that metals are present in the photospheres of almost all hot DA white dwarfs (e.g. Barstow et al. 1993, Marsh et al. 1997) due to radiative levitation (e.g. Chayer et al. 1994, Chayer et al. 1995). As first suggested by Dreizler & Werner (1993), the line blanketing caused by photospheric metals significantly affects  $T_{\text{eff}}$  measurements for DA white dwarfs with  $T_{\text{eff}} > 55000$  K (Barstow et al. 1998). Also, Barstow et al. (2001), Barstow et al. (2003) found that for  $T_{\text{eff}} > 50000$  K (the  $T_{\text{eff}}$  at which radiative levitation effects dominate and are responsible for putting metals into DA white dwarf photospheres) a significant difference between  $T_{\text{eff}}$  values derived from Balmer and Lyman line measurements arises (a similar effect is seen in DAO stars, Good et al. 2004). Uncertainties in modelling the metals in hot white dwarf photospheres (an analysis of the metal abundance patterns in hot DA white dwarfs shows that although the abundance patterns predicted by radiative levitation are broadly reproduced, the precise, measured abundances do not often match those predicted, Barstow et al. 2003) could go some way to explaining this phenomenon. Clearly, in light of the importance of accurate white

\* E-mail: njd15@le.ac.uk

dwarf  $T_{\text{eff}}$  measurements, a rigorous understanding of the metals in hot white dwarfs is required.

As well as the stratified hydrogen/helium configurations well known in many DAs (e.g. Vennes et al. 1988), evidence for stratified metal distributions (a phenomenon predicted by Chayer et al. 1995) has been seen in some stars. In a study of G191-B2B, Barstow et al. (1998) found an inhomogeneous iron distribution best fit the EUV, FUV and optical observations of the star, though the predicted and observed fluxes disagreed in the shortest wavelength regime ( $\lambda < 190 \text{ \AA}$ ). The stratified iron configuration was found to have an increasing abundance with depth; the iron depletion in the upper atmosphere was suggested to be a consequence of radiatively driven mass loss. Dreizler (1999) developed a method of modelling the EUV spectral region of hot white dwarfs, where the chemical abundance at each depth point was that produced by the equilibrium between radiative levitation and downward diffusion (with depth dependent radiation intensity). This gave a depth dependent abundance distribution, and successfully modelled the EUV spectrum of G191-B2B (Dreizler & Wolff 1999). A stratified nitrogen distribution was also used to simultaneously explain the FUV N V doublet (1238.82, 1242.80  $\text{\AA}$ ) and the observed EUV continuum in REJ 1032+532 (Holberg et al. 1999). Homogeneously distributed nitrogen with an abundance of  $N(N)/N(H)=5 \times 10^{-5}$  gave model line profiles with a depth similar to those observed, though they were pressure broadened beyond the observed profiles (figure 1, lower curve). Confining the nitrogen to a layer at the top of the atmosphere ( $\Delta M/M=3.1 \times 10^{-16}$ ) reduced this pressure broadening while maintaining the depth of the observed line profiles, better matching the data (figure 1, upper curve). The homogeneous nitrogen model caused heavy absorption of the EUV continuum (figure 2, lower curve); the lack of nitrogen in the lower atmosphere in the stratified model removed this absorber and reproduced the observed EUV continuum (figure 2, upper curve). Using *FUSE* observations of the O VI doublet (1031.912, 1037.613  $\text{\AA}$ ) and *EUVE* data, Chayer et al. (2006) found REJ 1032+532 to have a similarly stratified oxygen distribution (no interstellar O VI was observed by Barstow et al. 2010 to contaminate the photospheric O VI line profiles). Stratified nitrogen distributions similar to that of REJ 1032+532 were suggested to explain the N V doublet and EUV observations of GD 659 (Holberg et al. 1995; Barstow et al. 2003) and the N V doublet of REJ 1614-085 (Holberg et al. 1997; Holberg et al. 2000; Barstow et al. 2003). The analysis of Barstow et al. (2003) found that above 50000 K there was no pattern between nitrogen abundance and  $T_{\text{eff}}$ . Below 50000 K a dichotomy was observed, with the three white dwarfs discussed here forming a trend of increasing nitrogen abundance with decreasing  $T_{\text{eff}}$ , while definite nitrogen detections in the other white dwarfs could not be made (figure 3, black symbols).

Schuh et al. (2002) further developed and applied the stratified modelling method of Dreizler (1999) and Dreizler & Wolff (1999) to obtain metal abundances for a sample of stars. All stars were well fit with stratified metal distributions, save a few exceptions. Among these exceptions was REJ 1032+535 (= REJ 1032+532), which was better fit with a homogeneous metal distribution. A comparison by Schuh et al. (2005) of the abundances measured using the stratified modelling method of Schuh et al. (2002) (figure 3,

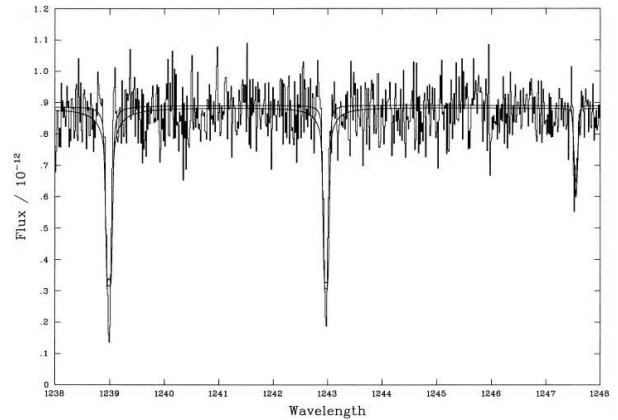


**Figure 1.** Figure 5 from Holberg et al. (1999). The N V doublet of REJ 1032+532 fit with a homogeneous model with  $N(N)/N(H)=5 \times 10^{-5}$  is represented by the lower curve. The upper curve is a model with stratified ( $\Delta M/M=3.1 \times 10^{-16}$ ) nitrogen (again,  $N(N)/N(H)=5 \times 10^{-5}$ ). A C III absorption feature is also seen near 1247.5  $\text{\AA}$ .

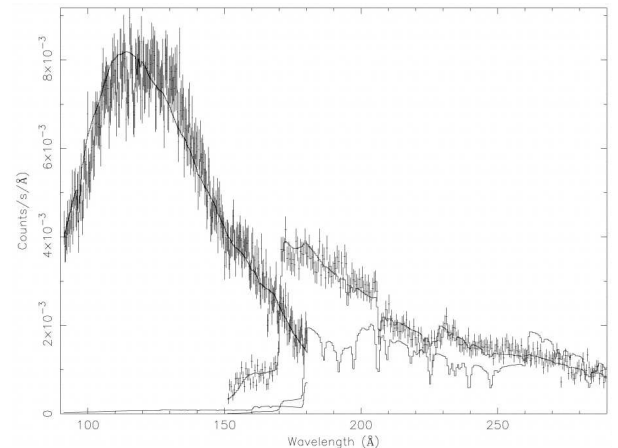


**Figure 2.** Figure 6 from Holberg et al. (1999). The data are the EUVE SW and MW EUV continuum of REJ 1032+532. The best fitting models for each dataset are the stratified nitrogen model. The other poorly fitting, heavily absorbed models are those with homogeneous nitrogen (again, a model is pictured for both the SW and MW data).

light grey symbols) to the measurements obtained from the homogeneous model grids of Barstow et al. (2003) (figure 3, black symbols) found that the nitrogen abundances for REJ 1032+532, REJ 1614-085 and GD 659 were much lower than those obtained by Barstow et al. (2003). The trend of increasing nitrogen abundance with decreasing  $T_{\text{eff}}$  observed by Barstow et al. (2003) was also not observed. Chayer et al. (2005) came to a similar conclusion (figure 4), though the measured abundances in this case were noticeably greater than those found by Schuh et al. (2005) in the cases of REJ 1614-085 and GD 659. Chayer et al. (2005) used both FUV and EUV data and homogeneous model grids calculated using the same method used by Barstow et al. (2003). Indeed, a remark made by Schuh (2005) was that it was of concern that both Barstow et al. (2003) and Chayer et al. (2005) obtained such different results using the same method.

Given the conflicting results outlined so far, a further analysis to better constrain the distribution and abundance of ni-

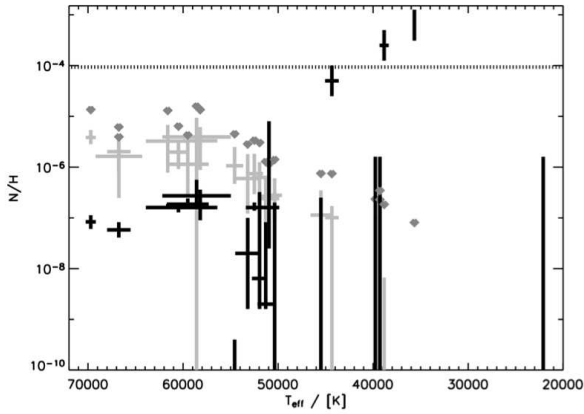


**Figure 3.** Figure 1 (third row, left hand panel) from Schuh et al. (2005). A comparison of the nitrogen abundances measured by Barstow et al. (2003) (black symbols) to the measurements of Schuh et al. (2005) (light grey symbols). The dark grey symbols show the radiative levitation predictions of Chayer et al. (1995) and the dotted line shows the cosmic abundance. Note that when non-detections of nitrogen were made by Barstow et al. (2003), an upper limit was estimated, leading to the large error bars seen in the black data points at lower  $T_{\text{eff}}$ .

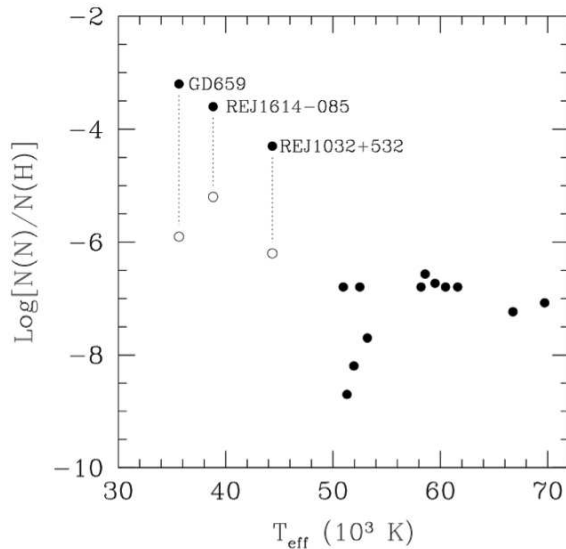


**Figure 4.** Figure 1 (left hand panel) from Chayer et al. (2005). A comparison of the nitrogen abundances measured by Barstow et al. (2003) (filled circles) to the measurements of Chayer et al. (2005) (open circles).

trogen in REJ 1032+532, REJ 1614-085 and GD 659 is desirable, and is presented here. The absorption line profiles of PG 0984+534 are extremely narrow and deep, akin to those of the REJ 1032+532 N V doublet. Barstow et al. (2003) stated that preliminary calculations suggested that the metals in the photosphere of the star was also stratified and, in light of the investigation into the photospheric nitrogen in REJ 1032+532, REJ 1614-085 and GD 659, PG 0948+534 is also investigated to see whether its enigmatic absorption line profiles can be modelled using stratified metal configurations.

## 2 OBSERVATIONS AND METHOD

The observations used in this work are detailed in table 1. Though the method applied here has been described in detail in previous work (e.g. Barstow et al. 2003), a summary is presented here. Models were computed using the non-LTE code TLUSTY (e.g. Hubeny & Lanz 1995). The  $T_{\text{eff}}$  and  $\log g$  values measured by Barstow et al. (2003) were used in the model calculations, and can be found in table 1 (along with the metal abundances measured by Barstow et al. 2003). The C, O, and Si abundances found by Barstow et al. (2003) were used in the model calculations of REJ 1032+532, REJ 1614-085 and GD 659 (where both C III and C IV abundances were found by Barstow et al. (2003), the higher abundance was included). Model atoms for C III, C IV, N III, N IV, N V, O IV, O V, O VI, Si III and Si IV were explicitly included, while C V, N VI, O VII and Si V were treated as one level atoms. The hydrogen broadening tables of Lemke (1997) were also included. Unlike the study of Barstow et al. (2003), which probed only the high nitrogen abundance regime, homogeneous model grids were constructed for each object to encompass the nitrogen abundances of both Barstow et al. (2003) and Chayer et al. (2005), to allow a full examination of the variation of the N V doublet line profile and EUV continuum with nitrogen abundance.

FUV spectra were synthesised from 1235Å to 1245Å to cover the N V doublet, and the XSPEC package was used to compare the model spectra to the observed data using a  $\chi^2$  minimisation technique. When a best fit nitrogen abundance was found, a set of stratified models were calculated, with the nitrogen abundance at the top of the atmosphere equal to the best fitting homogeneous abundance. Below this layer the nitrogen abundance was zero. In each model, the depth of this nitrogen layer was extended, allowing a model grid to be constructed to investigate whether a stratified metal configuration better matched the data (it must be stressed that the stratified models calculated here are not the self-consistently formulated, depth dependent models of the form of Dreizler 1999, Dreizler & Wolff 1999 and Schuh et al. 2002, but are ‘exploratory’ stratified models of the type computed by Barstow et al. 1998 and Holberg et al. 1999). The EUV analysis was conducted in the SW range (80 Å to 180 Å), since the EUV absorption was most severe there. Again, XSPEC was used to compare the models to the data. EUV interstellar absorption along the sight lines to the white dwarfs was accounted for using the column densities in table 1. The model grids used by Barstow et al. (2003) were used to fit the FUV absorption features (table 2) of PG 0948+534. After initial metal abundances were estimated, stratified grids were computed in the same way as the stratified nitrogen grids. The abundances of the metals other than the metal being stratified were fixed at the abundance estimates obtained using the homogeneous models computed by Barstow et al. (2003). The Fe and Ni abundances measured by Barstow et al. (2003) were included in all models of this object.

## 3 REJ 1032+532

An examination of the FUV N V doublet (1238.821, 1242.804 Å) found a global best fit for the homogeneous model at  $3.39 \pm_{1.31}^{1.29} \times 10^{-7}$ , with a  $\chi^2_{\nu} = 0.58$  (figure 5). A secondary best fit was found at  $5.00 \pm_{0.48}^{2.55} \times 10^{-5}$ , with a  $\chi^2_{\nu} = 0.77$ . Stratifying the model at either abundance did not improve the fit over the lower

**Table 1.** The observation information,  $T_{\text{eff}}$ ,  $\log g$ , metal abundances and ISM column densities towards the white dwarfs studied here. All observations, values of  $T_{\text{eff}}$ ,  $\log g$  and metal abundances are those detailed by Barstow et al. (2003), unless stated otherwise. The interstellar column densities are from the references indicated. The absence of data signifies where a measurement was unobtainable, either due to lack of spectral coverage in the required region or an inability to model absorption features.

	PG 0948+534	REJ 1032+532	REJ 1614-085	GD 659
FUV data	HST <i>STIS</i> [E140M]	HST <i>STIS</i> [E140M] <sup>a</sup>	HST <i>GHRs</i> [G160M] <sup>b</sup>	HST <i>STIS</i> [E140M]
EUV data		<i>EUVE</i> [SW] <sup>a</sup>		<i>EUVE</i> [SW] <sup>c</sup>
$T_{\text{eff}}$ (K)	110000	44350	38840	35660
$\log g$	7.58	7.81	7.92	7.93
$N(\text{C III})/N(\text{H})$		$3.00 \times 10^{-7}$		0.00
$N(\text{C IV})/N(\text{H})$		$1.60 \times 10^{-7}$	$7.00 \times 10^{-7}$	$5.00 \times 10^{-8}$
$N(\text{N V})/N(\text{H})$		$5.00 \times 10^{-5}$	$2.50 \times 10^{-4}$	$6.30 \times 10^{-4}$
$N(\text{N V})/N(\text{H})^d$		$1.26 \times 10^{-6}$	$6.31 \times 10^{-7}$	$6.31 \times 10^{-6}$
$N(\text{O V})/N(\text{H})$		$1.20 \times 10^{-7}$		0.00
$N(\text{Si IV})/N(\text{H})$		$9.50 \times 10^{-7}$	$9.50 \times 10^{-9}$	$4.80 \times 10^{-9}$
$N(\text{Fe V})/N(\text{H})$	$1.90 \times 10^{-6}$	0.00	0.00	0.00
$N(\text{Ni V})/N(\text{H})$	$1.20 \times 10^{-7}$	0.00	0.00	0.00
$\log(N_{\text{HI}})$ (cm <sup>-2</sup> )		18.62 <sup>e</sup>		18.46 <sup>f</sup>
$\log(N_{\text{HeI}})$ (cm <sup>-2</sup> )		17.75 <sup>e</sup>		17.37 <sup>f</sup>
$\log(N_{\text{HeII}})$ (cm <sup>-2</sup> )		17.28 <sup>e</sup>		17.17 <sup>f</sup>

<sup>a</sup>Holberg et al. (1999), <sup>b</sup>Holberg et al. (1997), <sup>c</sup>Holberg et al. (1995), <sup>d</sup>Chayer et al. (2005), <sup>e</sup>Holberg et al. (1999), <sup>f</sup>Barstow et al. (1997).

**Table 2.** The high ions examined in the spectrum of PG 0948+534 and their laboratory wavelengths

Ion	Lab. Wavelength (Å)
C IV	1548.187, 1550.772
N V	1238.821, 1242.804
O V	1371.296
Si IV	1393.755, 1402.770

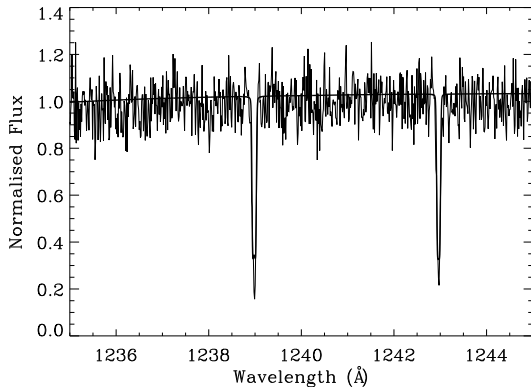


**Figure 5.** The FUV N V doublet of REJ 1032+532, fit with a homogeneous model with  $N(\text{N})/N(\text{H}) = 3.39 \times 10^{-7}$ .

abundance, homogeneous model. The lower abundance model fit the EUV data well (figure 6); no nitrogen absorption edge was seen in the SW data, where it had dominated in the high abundance homogeneous model of Holberg et al. (1999) (figure 2).

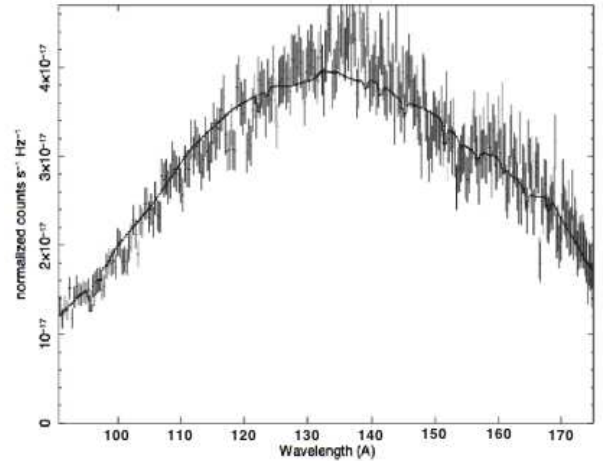


**Figure 6.** The homogeneous model of REJ 1032+532, with  $N(\text{N})/N(\text{H}) = 3.39 \times 10^{-7}$ , fit to the *EUVE* SW data.

#### 4 REJ 1614-085

A lower nitrogen abundance secondary best fit was found at  $1.76 \pm_{1.26}^{1.65} \times 10^{-6}$  ( $\chi^2_{\nu} = 1.21$ ) (figure 7, upper panel). Unlike REJ 1032+532, the analysis of the FUV N V doublet of this DA found a best fitting abundance in the high abundance regime, at  $3.41 \pm_{1.50}^{1.81} \times 10^{-4}$  ( $\chi^2_{\nu} = 1.13$ ) (figure 7, lower panel). The lower abundance model here over predicted the depths of the observed line profiles, while the absorption lines of the higher abundance model did not quite extend into the observed line profiles. An explanation of this behaviour and the degeneracy in the previous star is presented in section 7.

#### 5 GD 659

In keeping with REJ 1032+532, two best fitting abundances were found for GD 659, with the overall best fitting abundance



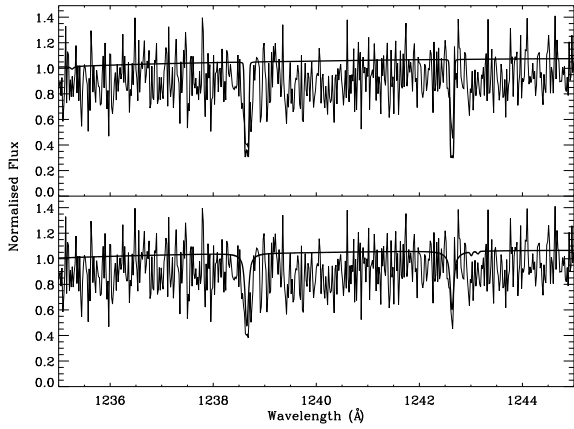


**Figure 7.** The lower abundance model ( $1.76 \times 10^{-6}$ ;  $\chi^2_v = 1.21$ ) of REJ 1614-085 is in the upper panel. The high nitrogen abundance model ( $3.41 \times 10^{-4}$ ;  $\chi^2_v = 1.13$ ) is shown in the lower panel.

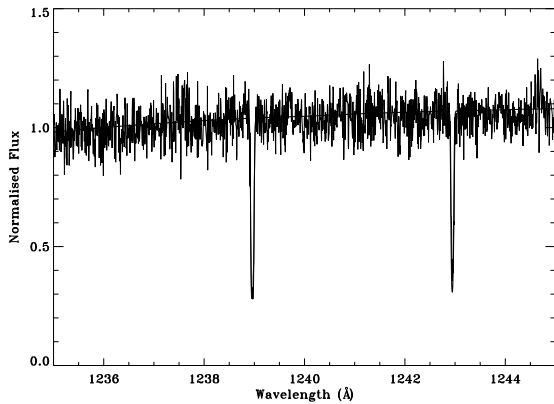


**Figure 8.** The FUV N V doublet of GD 659, fit with a homogeneous model with  $N(N)/N(H) = 6.05 \times 10^{-7}$ .

at  $6.05 \pm_{0.62}^{0.64} \times 10^{-7}$  ( $\chi^2_v = 2.15$ ; figure 8) and the secondary best fitting abundance at  $5.70 \pm_{0.62}^{0.41} \times 10^{-5}$  ( $\chi^2_v = 2.41$ ). Again, stratifying the high abundance model did not offer a better fit to the data than the lower abundance, homogeneous model. Like REJ 1032+532, no nitrogen absorption edge was seen at EUV wavelengths at the lower, homogeneous abundance.

## 6 PG 0948+534

The absorption line profiles in the spectrum of PG 0948+534 could not be modelled satisfactorially here (figure 9). The best fitting, homogeneous C IV abundance was found to be  $4.85 \times 10^{-6}$ , while the N V doublet, O V line and Si IV doublet were best fit with abundances of  $1.6 \times 10^{-6}$ ,  $3.5 \times 10^{-5}$  (the O V grid upper limit of 100 times the abundance of G191-B2B) and  $3.15 \times 10^{-5}$ , respectively. Above these abundances, the depth of the line profiles could not be reproduced while maintaining the narrow width of the lines. Stratifying the metals did not improve the fits. Given the poor match to the data provided by these models, errors were not computed for these measurements.

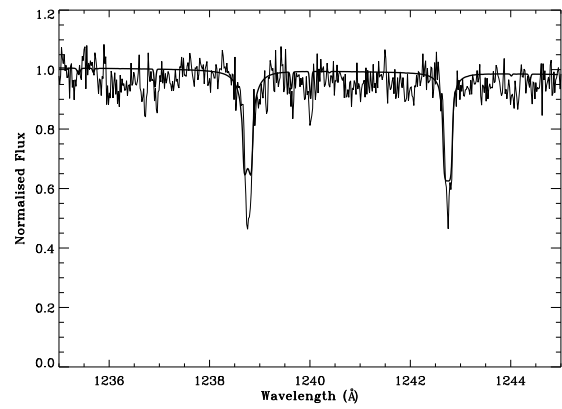


**Figure 9.** The N V doublet of PG 0948+534, fit with a model with a nitrogen abundance of  $1.60 \times 10^{-6}$ .

**Table 3.** The nitrogen abundances for REJ 1032+532, REJ 1614-085 and GD 659.

Star	$N(N)/N(H)$	+3 $\sigma$	-3 $\sigma$
REJ 1032+532	$3.39 \times 10^{-7}$	$1.29 \times 10^{-7}$	$1.31 \times 10^{-7}$
REJ 1614-085	$1.76 \times 10^{-6}$	$1.65 \times 10^{-7}$	$1.26 \times 10^{-7}$
GD659	$6.05 \times 10^{-7}$	$0.64 \times 10^{-7}$	$0.62 \times 10^{-7}$

## 7 DISCUSSION

A degeneracy was seen in the modelling of photospheric nitrogen in REJ 1032+532, REJ 1614-085 and GD 659. The best fitting abundances for each star are presented in table 3 (the results for PG 0948+534 are not included as they are thought not to be reliable). Figure 10 shows the  $\chi^2_v$  distribution of REJ 1032+532 as nitrogen abundance was increased. The upper panel shows that as  $N(N)/N(H)$  is increased, two minima are seen at the best fitting abundances of  $3.39 \times 10^{-7}$  and  $5 \times 10^{-5}$ . The lower panel shows the minima in more detail, with the dashed line representing the global minimum in  $\chi^2_v$  (0.58) and the dotted line showing the 3 $\sigma$  confidence limit of this minimum. The secondary minimum ( $\chi^2_v = 0.77$ ) is clearly separated from the confidence limit of the global minimum, so the global minimum can confidently be declared the best fitting abundance. The lower abundance model also fit the *EUVE* SW data well. A similar situation occurs for GD 659, with a best fit abundance of  $6.05 \pm_{0.62}^{0.64} \times 10^{-7}$ .

In REJ 1614-085, the two minima are less easy to disentangle. The lower panel of figure 11 shows that the separation of the two minima is not greater than the 3 $\sigma$  confidence limit of the global minimum. Indeed, the higher nitrogen abundance ( $3.41 \pm_{1.50}^{1.81} \times 10^{-4}$ ) is, marginally, the global minimum. A close inspection of the  $\chi^2_v$  distribution shows that poorly defined minima are also present near  $N(N)/N(H) = 10^{-5}$  (figure 11, upper panel) and  $7 \times 10^{-3}$  (figure 11, lower panel). Given that both REJ 1032+532 and GD 659 are well explained with lower nitrogen abundance, homogeneous models and that the minima in the  $\chi^2_v$  distribution of REJ 1614-085 cannot be confidently disentangled, the lower nitrogen abundance ( $1.76 \pm_{1.26}^{1.65} \times 10^{-6}$ ) is deemed the best fit here. Better signal-to-noise data may help to break this degeneracy with more confidence, and may allow a better match to the observed line profiles. In PG 0948+534, the  $\chi^2_v$  distributions for C IV, N V, O V and Si IV have single minima. The

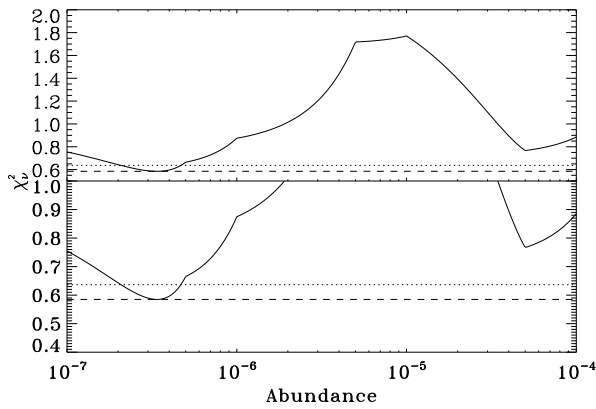


**Figure 10.** The  $\chi_v^2$  distribution of REJ 1032+532 as nitrogen abundance increased. The global  $\chi_v^2$  minimum is represented with a dashed line, and its  $3\sigma$  confidence limit is denoted with a dotted line.

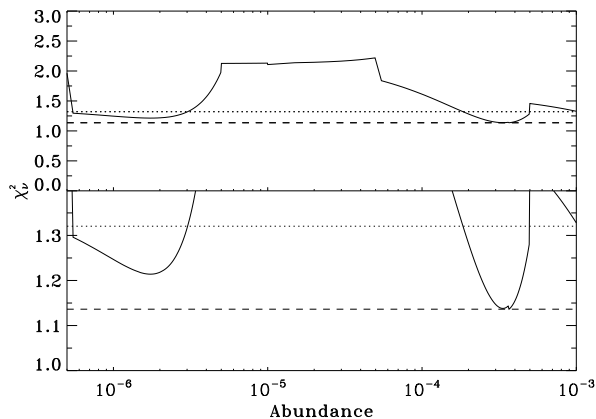


**Figure 11.** The  $\chi_v^2$  distribution of REJ 1614-085. Again, the global  $\chi_v^2$  minimum is represented with a dashed line, and its  $3\sigma$  confidence limit is denoted with a dotted line.

values of  $\chi_v^2$  were high (with values of 2.9-9.8 across the high ion fits), showing that the models used here do not appropriately represent the metal absorption seen in this star.

A comparison of the model NLTE population responsible for the N V doublet absorption ( $^2S$ ) to the N VI level shows that at high nitrogen abundances, the value of  $\log(N V(^2S)/N VI)$  decreases above nitrogen abundances  $\sim 10^{-6}$  (figure 12). Note that not all the model grids cover the same abundance range, only the range required to explain the observed line profiles in each case. This ‘over-ionisation’ may provide a mechanism for the apparent degeneracy; although the nitrogen abundance in each case is increasing, the relative amount of N V ( $^2S$ ) decreases. Given that  $\log(N V(^2S)/N VI)$  of REJ 1614-085 follows the same trend as the  $\log(N V(^2S)/N VI)$  of both REJ 1032+532 and GD 659, this further suggests that though the degeneracy seen in figure 11 cannot be confidently broken, REJ 1614-085 has a homogeneous nitrogen distribution with an abundance in keeping with the other objects.

The work (e.g. Holberg et al. 1999) that found the nitrogen in these stars to be stratified and of high abundance cite a radiatively driven mass loss process as the reason for the nitrogen distribution. Recent studies looking at mass loss in

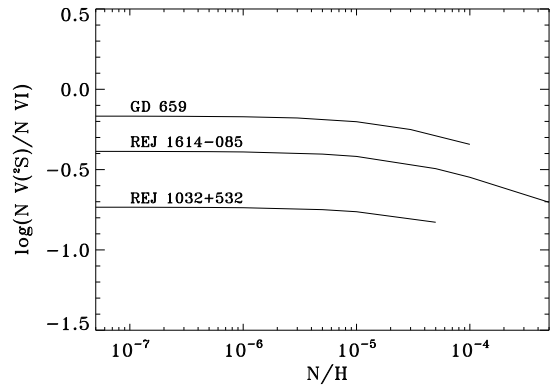
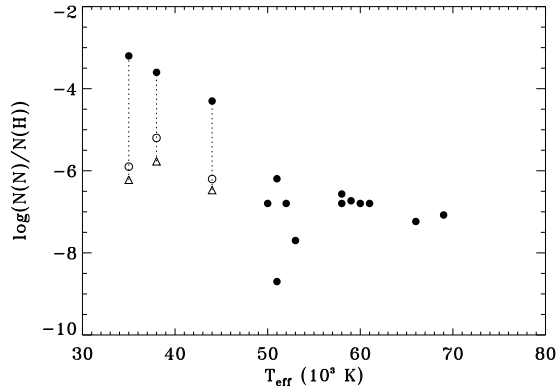


**Figure 12.** The change in the log of the ratio of the N V NLTE populations responsible for the N V doublet to the N VI level population in the stellar models, with nitrogen abundance.

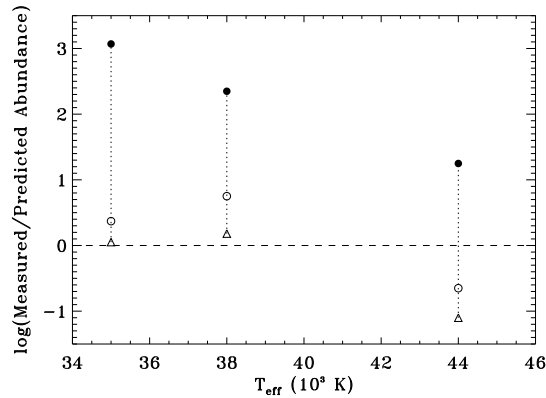
DA white dwarfs have found that for DAs in the 25000 K  $< T_{\text{eff}} < 50000$  K range, mass loss cannot occur for stars with  $\log g > 7.0$  since the upward radiative pressure cannot overcome the gravity of the star (Unglaub 2008). Indeed, even up to and beyond  $T_{\text{eff}} = 60000$  K, mass loss cannot occur for DAs with  $\log g > 7.0$  (Unglaub & Bues 2000, Unglaub 2007). No circumstellar N V has been found at these objects, from which accretion can take place and enrich the upper atmosphere (Bannister et al. 2003, Dickinson et al. 2012). This suggests that the nitrogen enrichment in the upper atmosphere due to either mass loss or accretion cannot be happening, strengthening the argument for a homogeneous nitrogen distribution in all of the objects.

Figure 13 shows a comparison of the nitrogen abundances found here (triangular symbols) to those found by Barstow et al. (2003) (filled circles) and Chayer et al. (2005) (open circles). The nitrogen abundances measured here are more in keeping with the nitrogen abundances measured by Barstow et al. (2003) for DA white dwarfs of higher  $T_{\text{eff}}$ . The pattern between nitrogen abundance and  $T_{\text{eff}}$  seen by Chayer et al. (2005) is reproduced, though the measured abundances here are offset to those measured by Chayer et al. (2005) (probably due to systematic differences in the fitting procedures used by Chayer et al. 2005 when compared to the method here). The trend of increasing nitrogen abundance seen by Barstow et al. (2003) is not seen here. A comparison of the results for REJ 1032+532, REJ 1614-085 and GD 659 to the radiative levitation predictions of Chayer et al. (1995) (figure 14) shows that the abundances derived here are much closer to those those predicted by radiative levitation theory than those found by Barstow et al. (2003).

In view of the fact that the low nitrogen abundance models were preferred over the high nitrogen abundance models in the cases of REJ 1032+532, REJ 1614-085 and GD 659, it was perhaps no surprise that stratified model calculations also failed to explain the high ion absorption features of PG 0948+534. The much higher  $T_{\text{eff}}$  of PG 0948+534 (being 65650 K hotter than the next hottest star, REJ 1032+532) may introduce some physical effects that are not accounted for in the models. Another possible reason for the observed line profiles in this object is the presence of unresolved material along the sight line of the white



**Figure 13.** A comparison of the nitrogen abundances found here (triangles) to those found by Barstow et al. (2003) (filled circles) and Chayer et al. (2005) (open circles). The dotted lines connect the data points of a given star to aid comparison.



**Figure 14.** A comparison of the abundances found here, by Barstow et al. (2003) and by Chayer et al. (2005) to those predicted by Chayer et al. (1995). The plot symbols are the same as for figure 13

dwarf at a velocity co-incident with the photosphere. This will be explored in a later paper.

## ACKNOWLEDGEMENTS

NJD and MAB acknowledge the support of STFC. NJD wishes to thank Klaus Unglaub and Matt Burleigh for useful discussions.

## REFERENCES

Bannister N., Barstow M., Holberg J., Bruhweiler F., 2003, MNRAS, 341, 477  
 Barstow M., Boyce D., Welsh B., Lallement R., Barstow J., Forbes A., Preval S., 2010, ApJ, 723, 1762  
 Barstow M., Dobbie P., Holberg J., Hubeny I., Lanz T., 1997, MNRAS, 286, 58  
 Barstow M., Fleming T., Diamond C., Finley D., Sansom A., Rosen S., Koester D., Holberg J., Marsh J., Kidder K., 1993, MNRAS, 264, 16

Barstow M., Good S., Burleigh M., Hubeny I., Holberg J., Levan A., 2003, MNRAS, 344, 562  
 Barstow M., Good S., Holberg J., Hubeny I., Bannister N., Bruhweiler F., Burleigh M., Napiwotzki R., 2003, MNRAS, 341, 870  
 Barstow M., Good S., Holberg J., Hubeny I., Bannister N., Bruhweiler F., Burleigh M., Napiwotzki R., 2003, MNRAS, 341, 870  
 Barstow M., Holberg J., Hubeny I., Good S., Levan A., F. M., 2001, MNRAS, 328, 211  
 Barstow M., Hubeny I., Holberg J., 1998, MNRAS, 299, 520  
 Bergeron P., Saffer R., Liebert J., 1992, ApJ, 432, 305  
 Casewell S., Dobbie P., Napiwotzki R., Burleigh M., Barstow M., Jameson R., 2009, MNRAS, 395, 1795  
 Chayer P., LeBlanc F., Fontaine G., Wesemael F., Michaud G., Vennes S., 1994, ApJ, 436, 161  
 Chayer P., Oliveira C., Dupuis J., Moos H., Welsh B., 2006, ASPC, 348, 209  
 Chayer P., Vennes S., Dupuis J., 2005, ASPC, 334, 181  
 Chayer P., Vennes S., Pradhan A., Thejll P., Beauchamp A., Fontaine G., Wesemael F., 1995, ApJ, 454, 429  
 Dickinson N., Barstow M., Welsh B., Burleigh M., Farihi J., Redfield S., Unglaub K., 2012, in prep  
 Dobbie P., Napiwotzki R., Burleigh M., Williams K., Sharp R., Barstow M., Casewell S., Hubeny I., 2009, MNRAS, 395, 2248  
 Dreizler S., 1999, A&A, 352, 632  
 Dreizler S., Werner K., 1993, A&A, 278, 199  
 Dreizler S., Wolff B., 1999, A&A, 348, 189  
 Fontaine G., Brassard P., Bergeron P., 2001, PASP, 113, 409  
 Good S., Barstow M., Holberg J., Sing D., Burleigh M., Dobbie P., 2004, MNRAS, 355, 1031  
 Holberg J., Barstow M., Bruhweiler F., Dobbie P., 1999, ApJ, 517, 841  
 Holberg J., Barstow M., Bruhweiler F., Hubeny I., 2000, American Astron. Soc. Meeting, 197, 8304  
 Holberg J., Barstow M., Bruhweiler F., Hubeny I., Green E., 1999, ApJ, 517, 850  
 Holberg J., Barstow M., Bruhweiler F., Sion E., 1995, ApJ, 453, 313  
 Holberg J., Barstow M., Lanz T., Hubeny I., 1997, ApJ, 484, 871  
 Holberg J., Wesemael F., Wegner G., Bruhweiler F., 1985, ApJ, 293, 294  
 Hubeny I., Lanz T., 1995, ApJ, 439, 875  
 Lemke M., 1997, A&AS, 122, 285  
 Liebert J., Bergeron P., Holberg J., 2005, ApJS, 156, 47  
 Marsh M., Barstow M., Burleigh M., Holberg J., Koester D., O'Donoghue D., Penny A., Sansom A., 1997, MNRAS, 287, 705  
 Schuh S., 2005, PhD Thesis  
 Schuh S., Barstow M., Dreizler S., 2005, ASPC, 334, 237  
 Schuh S., Dreizler S., Wolff B., 2002, A&A, 382, 164  
 Unglaub K., 2007, ASPC, 372, 201  
 Unglaub K., 2008, A&A, 486, 923  
 Unglaub K., Bues I., 2000, A&A, 359, 1042  
 Vennes S., Pelletier C., Fontaine G., Wesemael F., 1988, ApJ, 331, 876  
 Wood M., 1995, LNP, 443, 41